



**HAL**  
open science

# The deep atmosphere of Venus and the possible role of density-driven separation of CO<sub>2</sub> and N<sub>2</sub>

Sébastien Lebonnois, Gerald Schubert

► **To cite this version:**

Sébastien Lebonnois, Gerald Schubert. The deep atmosphere of Venus and the possible role of density-driven separation of CO<sub>2</sub> and N<sub>2</sub>. *Nature Geoscience*, 2017, 10 (7), pp.473 - 477. 10.1038/ngeo2971 . hal-01635402

**HAL Id: hal-01635402**

**<https://hal.science/hal-01635402>**

Submitted on 15 Nov 2017

**HAL** is a multi-disciplinary open access archive for the deposit and dissemination of scientific research documents, whether they are published or not. The documents may come from teaching and research institutions in France or abroad, or from public or private research centers.

L'archive ouverte pluridisciplinaire **HAL**, est destinée au dépôt et à la diffusion de documents scientifiques de niveau recherche, publiés ou non, émanant des établissements d'enseignement et de recherche français ou étrangers, des laboratoires publics ou privés.

# The deep atmosphere of Venus and the possible role of density-driven separation of CO<sub>2</sub> and N<sub>2</sub>

Sebastien Lebonnois,<sup>1\*</sup> Gerald Schubert<sup>2</sup>

<sup>1</sup>Laboratoire de Météorologie Dynamique (LMD/IPSL),  
Sorbonne Universités, UPMC Univ Paris 06, ENS, PSL Research University,  
Ecole Polytechnique, Université Paris Saclay, CNRS, Paris, France

<sup>2</sup>Department of Earth, Planet. and Space Sci., UCLA, CA, USA

\*e-mail: [sebastien.lebonnois@lmd.jussieu.fr](mailto:sebastien.lebonnois@lmd.jussieu.fr).

1     **With temperatures around 700 K and pressures of around 75 bar, the deepest**  
2     **12 kilometres of the atmosphere of Venus are so hot and dense that the atmo-**  
3     **sphere behaves like a supercritical fluid. The Soviet VeGa-2 probe descended**  
4     **through the atmosphere in 1985 and obtained the only reliable temperature**  
5     **profile for the deep Venusian atmosphere thus far. In this temperature profile,**  
6     **the atmosphere appears to be highly unstable at altitudes below 7 km, con-**  
7     **trary to expectations. We argue that the VeGa-2 temperature profile could be**  
8     **explained by a change in the atmospheric gas composition, and thus molec-**  
9     **ular mass, with depth. We propose that the deep atmosphere consists of a**  
10    **non-homogeneous layer in which the abundance of N<sub>2</sub> - the second most abun-**  
11    **dant constituent of the Venusian atmosphere after CO<sub>2</sub> - gradually decreases**  
12    **to near-zero at the surface. It is difficult to explain a decline in N<sub>2</sub> towards the**  
13    **surface with known nitrogen sources and sinks for Venus. Instead we suggest,**

14 **partly based on experiments on supercritical fluids, that density-driven sep-**  
15 **aration of N<sub>2</sub> from CO<sub>2</sub> can occur under the high pressures of Venus's deep**  
16 **atmosphere, possibly by molecular diffusion, or by natural density-driven con-**  
17 **vection. If so, the amount of nitrogen in the atmosphere of Venus is 15% lower**  
18 **than commonly assumed. We suggest that similar density-driven separation**  
19 **could occur in other massive planetary atmospheres.**

20 Venus has a massive and scorching atmosphere. With a surface pressure of 92 bars its atmo-  
21 sphere is 92 times as massive as Earth's atmosphere. At the surface of Venus the temperature  
22 is 464°C, hot enough to melt lead. Atmospheric density at the surface is about 65 kg m<sup>-3</sup> or  
23 6.5% the density of liquid water.<sup>1</sup> Atmospheric composition is 96.5% CO<sub>2</sub> and 3.5% N<sub>2</sub> (by  
24 volume).<sup>2</sup> Minor gases include SO<sub>2</sub>, Ar, H<sub>2</sub>O, and CO.<sup>3,4</sup> SO<sub>2</sub> at the level of only 150 ppm is  
25 particularly important because of the blanket of sulfuric acid clouds that completely shroud the  
26 planet from view.<sup>5</sup> The clouds effectively reflect the solar radiation incident on Venus resulting  
27 in a bond albedo of 0.77, more than double that of the Earth at 0.31. As a consequence more  
28 sunlight is absorbed at the surface of Earth than at Venus' surface even though Venus is 72%  
29 nearer to the Sun. The temperature distribution in Venus' atmosphere is determined in large  
30 part by its absorption of sunlight.<sup>1</sup> Temperature and pressure are so large at Venus' surface that  
31 the atmosphere is a supercritical fluid.

32 In addition to the basic properties above we have detailed knowledge of the atmospheric  
33 structure (altitude profiles of temperature and pressure and locations of the clouds) from decades  
34 of observation by orbiting spacecraft (Soviet Venera 15 and 16,<sup>6-8</sup> U.S. Pioneer Venus Or-  
35 biter<sup>9,10</sup> and Magellan,<sup>11</sup> ESA Venus-Express<sup>12-14</sup> and the ongoing Japanese Akatsuki), entry  
36 probes and landers,<sup>15-18</sup> balloons,<sup>17</sup> and Earth-based telescopes<sup>3,19-21</sup> (Fig. 1). These obser-  
37 vations have shown that Venus, like Earth, has a troposphere extending from the surface to the  
38 upper cloud region at about 60 to 65 km altitude, wherein temperature decreases with height.<sup>1,22</sup>

39 The sulfuric acid clouds extend downward to about 48 km altitude.<sup>5</sup> Above the clouds are re-  
40 gions of the atmosphere analogous to Earth's mesosphere and thermosphere but our focus here  
41 is the atmosphere below the clouds. At cloud heights atmospheric temperature and pressure  
42 are similar to those at the Earth's surface. There is no stratosphere on Venus similar to Earth's  
43 stratosphere that is heated by ozone absorption of solar ultraviolet radiation.

44 The altitude profile of temperature allows identification of stable layers and layers of convec-  
45 tive activity. There is a convective region in the clouds between about 50 and 55 km altitude,<sup>14,23</sup>  
46 as experienced by the Soviet VeGa-1 and VeGa-2 balloons that cruised in this layer.<sup>17</sup> Below  
47 this region extending downward to about 32 km altitude the atmosphere is stable. Below this  
48 stable layer the atmosphere is well mixed down to an altitude of about 18 km. At even greater  
49 depth, the atmosphere is stable again until an altitude of about 7 km. The nature of the lowest  
50 7 km of the atmosphere, a layer that contains 37% of the mass of the atmosphere, is at the heart  
51 of our discussion.

52 While the exploration of Venus' atmosphere has been extensive, as discussed above, the  
53 deep atmosphere remains a largely unobserved region. It is challenging to obtain data remotely  
54 below the thick cloud layer covering the planet. Many probes have been sent to the surface  
55 of Venus: the Soviet Venera mission series,<sup>15</sup> the U.S. Pioneer Venus probes,<sup>16</sup> and the Soviet  
56 VeGa probes.<sup>17,18</sup> These probes measured temperature ( $T$ ) and pressure ( $p$ ) during descent, and  
57 made measurements of atmospheric composition, showing that the two major constituents were  
58 carbon dioxide (CO<sub>2</sub>, 96.5%) and nitrogen (N<sub>2</sub>, 3.5%).<sup>2,24,25</sup> Unfortunately, almost no tem-  
59 perature data were obtained from the deepest layers of Venus' atmosphere, since most Venera  
60 probe temperature profiles had large uncertainties and all the Pioneer Venus probe temperature  
61 experiments stopped functioning at 12 km above the surface.<sup>22</sup> The Pioneer Venus tempera-  
62 ture profiles below 12 km were reconstructed from pressure measurements, extrapolation of  
63  $T(p)$  and iterative altitude computation,<sup>16</sup> and only these reconstructions (prone to significant

64 uncertainties) and the Venera 10 profile<sup>26</sup> were used to build the Venus International Reference  
65 Atmosphere model.<sup>22</sup> The only available and reliable temperature profile reaching to the surface  
66 was acquired by the VeGa-2 probe<sup>17,18,27</sup> (Fig. 2). Measurements were done with two different  
67 platinum wires (one bare, one protected in a thin ceramic shield), with a measured accuracy  
68 of  $\pm 0.5$  K from 200 to 800 K. The time constants of the two detectors were 0.1 s and 3 s.  
69 The delay of the second detector induced systematic shift between the two measurements, with  
70 differences no larger than 2 K down to the surface.<sup>17</sup> The measured temperature profile fits re-  
71 markably well with the Pioneer Venus and VIRA profiles above roughly 15 km altitude.<sup>27</sup> This  
72 illustrates the small temporal and spatial variability of the temperature in the deep atmosphere  
73 of Venus, with differences between the different observed profiles smaller than 5 K (and not  
74 depending on altitude).

75 Below 7 km, a region where no precise measurements of N<sub>2</sub> abundance was published,<sup>2</sup>  
76 the VeGa-2 temperature profile showed a strongly unstable vertical temperature gradient that  
77 has remained unexplained since VeGa-2 landed on Venus on June 15, 1985.<sup>27,28</sup> The difference  
78 in temperature between the adiabatic profile (neutral stability) and the observed profile is up  
79 to roughly 9 K around 7 km. This interface region between the surface and the atmosphere,  
80 called the planetary boundary layer (PBL), controls how the angular momentum and energy  
81 are exchanged between the two reservoirs. Characterization of the mixing processes occurring  
82 in the PBL is crucial to understanding the angular momentum budgets of the atmosphere and  
83 solid planet. This is particularly true in the case of Venus, which is characterized by a peculiar  
84 atmospheric circulation, the superrotation: the whole atmosphere is rotating much faster than  
85 the surface below, with maximum zonal winds reaching more than 100 m/s at the altitude of the  
86 cloud top (70 km).<sup>29</sup> This large zonal rotation of the massive Venus atmosphere makes its atmo-  
87 spheric angular momentum a relatively large fraction ( $1.6 \times 10^{-3}$ ) of the angular momentum of  
88 the solid body. For Earth this fraction is  $2.7 \times 10^{-8}$ . Exchanges of angular momentum between

89 the two reservoirs would lead to changes in the length of day of Venus and zonal wind speeds  
90 in the atmosphere.

91 A possible interpretation of this peculiar temperature structure involves unexpected proper-  
92 ties of the CO<sub>2</sub>/N<sub>2</sub> mixture in high-pressure, high-temperature conditions, which are not well  
93 known. This is illustrated by a recent experiment that shows a vertical separation between  
94 these two compounds within the fluid phase, a behavior difficult to explain.<sup>30</sup> Despite a lack  
95 of theoretical and experimental constraints, this density-driven separation may be the key to  
96 understanding the structure of the deepest layers of Venus' atmosphere.

## 97 **Stability in the deep atmosphere of Venus**

98 The temperature profile close to the surface is a very good indicator of the properties of the PBL.  
99 In addition to the static stability, the potential temperature is an efficient variable to analyze the  
100 stratification of the atmosphere (Box 1). The vertical profiles of the potential temperature de-  
101 rived from the VeGa-2 and Pioneer Venus probes are displayed in Fig. 3. Layers with constant  
102 potential temperature are layers where the temperature follows the adiabatic lapse rate, indica-  
103 tive of convection or large-scale vertical mixing. Below roughly 7 km, the vertical gradient of  
104 the VeGa-2 potential temperature is approximately constant and strongly negative (-1.5K/km),  
105 corresponding to a highly unstable situation. Such a profile of potential temperature is never  
106 observed on Earth. On Mars, radiative surface heating sometimes drives a very unstable surface  
107 layer, yielding highly active convection up to 9 km above surface. In these conditions, the po-  
108 tential temperature may display negative gradients over the surface, up to 1 or 2 km altitude.<sup>31</sup>  
109 For Venus, this situation is unlikely, as direct heating of the surface is only a small fraction of  
110 that of Mars' surface.<sup>32</sup>

111 However, the VeGa-2 probe potential temperature profile can be understood if the stability of  
112 this layer is altered by a vertical gradient in the mean molecular mass ( $\mu$ ), i.e., in the atmospheric

113 gas composition (as detailed in the online Methods section): the assumption that this layer is  
114 close to convective instability yields a vertical profile of mean molecular mass which is almost  
115 linear with the logarithm of pressure, from 43.44 g/mol above 7 km to 44.0 g/mol at the surface.

## 116 **A density-driven gas separation hypothesis**

117 Though a systematic error in the temperature measurements can not be excluded, the fact that  
118 this error would have maintained a stable vertical temperature gradient from 7 km altitude to  
119 the surface, for both VeGa-2 temperature sensors is unlikely. If this temperature profile is  
120 accurate, then it may be neutrally stable with the previously mentioned variation in the mean  
121 molecular mass  $\mu$ . The value obtained in this case for  $\mu$  at the surface is remarkably close  
122 to that of pure CO<sub>2</sub>, so that an intriguing, but very simple explanation for the vertical profile  
123 of  $\mu$  is a regular decrease in N<sub>2</sub> mole fraction, from 3.5% above 7 km to almost zero at the  
124 surface. Such a composition variation would have a significant impact on the total amount of  
125 nitrogen contained in the atmosphere, which would decrease to only 85% of the total amount for  
126 a well mixed atmosphere. This could have potential implications for studies that investigate the  
127 respective nitrogen inventories of Earth and Venus.<sup>33</sup> The increase of the mean molecular mass  
128 towards the surface might also be consistent with an increase in the abundance of an atmospheric  
129 compound heavier than CO<sub>2</sub>, though this would be an even more puzzling coincidence. For an  
130 increase up to the 0.1% level at the surface, the molar mass of the component would need to  
131 be of the order of 560 g/mol. A lower molar mass would mean a higher abundance. Solutions  
132 could be found, but it seems quite unlikely that the change of composition would be different  
133 from the decrease of N<sub>2</sub> abundance as the surface is approached.

134 Based on this hypothetical interpretation of the VeGa-2 probe temperature profile, the gra-  
135 dient in N<sub>2</sub> abundance obtained in Venus's deep atmosphere is around 5 ppm/m. In planetary  
136 atmospheres, such vertical gradients of composition are usually associated with sources or sinks

137 of the varying compound, such as chemistry, condensation, or surface processes. However, the  
138 hypothesis that this nitrogen gradient might be the result of a surface sink faces serious diffi-  
139 culties. It would require a constant downward flux of nitrogen, that would need to be sustained  
140 over geological times unless a recycling process or an equivalent source could drive nitrogen  
141 back into the atmosphere.

142 Another possibility is explored here : this gradient may result from an equilibrium state due  
143 to separation of nitrogen from carbon dioxide in the dense conditions of Venus's deep atmo-  
144 sphere. Such a separation of N<sub>2</sub> and CO<sub>2</sub> in high-pressure conditions is illustrated by recent ex-  
145 periments.<sup>30,34</sup> Though the conditions of these experiments are clearly different from conditions  
146 in the deep atmosphere of Venus, it demonstrates the impact of high densities on the CO<sub>2</sub>/N<sub>2</sub>  
147 binary mixture. In the first of these experiments,<sup>30</sup> a mixture of 50% N<sub>2</sub>/50% CO<sub>2</sub> (mole frac-  
148 tions) was put in an 18-cm high vessel at room temperature for pressures above 100 bars. At  
149  $p = 100$  bars and  $T = 23^\circ\text{C}$ , the CO<sub>2</sub>/N<sub>2</sub> mixture is supercritical, not far above the critical  
150 point of the fluid mixture ( $T_C = -9.3^\circ\text{C}$ ,  $p_C = 98$  bar), and CO<sub>2</sub> departs slightly from being  
151 ideal. Using the equations of state for pure CO<sub>2</sub> and N<sub>2</sub>,<sup>34,35</sup> CO<sub>2</sub> partial pressure is 44 bars,  
152 CO<sub>2</sub> density is 101 kg/m<sup>3</sup> and total density in the vessel is around 165 kg/m<sup>3</sup>, to be compared  
153 with the densities in the deep Venusian atmosphere: 40 to 70 kg/m<sup>3</sup> for pressures higher than  
154 50 bars. In these experimental conditions, N<sub>2</sub> and CO<sub>2</sub> were observed to separate significantly  
155 along the vertical dimension, N<sub>2</sub> reaching over 70% mole fraction at the top of the vessel, while  
156 CO<sub>2</sub> reached almost 90% at the bottom.<sup>30</sup> Over the 18 cm of the experimental vessel, this sep-  
157 aration is extreme, with an average gradient of 3 to 4%/cm. In Venus's deep atmosphere, the  
158 5 ppm/m gradient in N<sub>2</sub> abundance appears much smaller in comparison.

159 The molecular diffusion in this binary gas mixture includes three terms: one due to the  
160 compositional gradient, one due to the temperature gradient, and one due to the pressure gra-  
161 dient.<sup>36</sup> The amplitude of this pressure term is controlled by the barodiffusion coefficient  $k_p$ .



162 Molecular diffusion in an ideal gas mixture increases as the pressure decreases towards higher  
163 altitudes, the expression of  $k_p$  is known for an ideal binary gas mixture, and turbulent diffusion  
164 in usual atmospheric conditions is strong enough to homogenize atmospheric composition up to  
165 the homopause. At this level, molecular diffusion dominates and the barodiffusion induces mass  
166 separation of the different compounds. Could high-pressure conditions and departure from the  
167 ideal gas law induce strongly non-linear behavior of the barodiffusion coefficient ? For such  
168 a gradient to be maintained in the near-surface layer of Venus's atmosphere against large-scale  
169 and turbulent mixing, the barodiffusion coefficient  $k_p$  would need to be several orders of mag-  
170 nitude larger than for an ideal gas in the same conditions, which may seem highly unlikely. It  
171 is also the case for the previously detailed experiment.<sup>30</sup> Unfortunately, no measured or theo-  
172 retical values are yet available for  $k_p$ , neither for the experimental set-up<sup>30</sup> nor for Venus's deep  
173 atmospheric conditions. In the experiments,<sup>30,34</sup> natural density-driven convection is mentioned  
174 as a possible driver, inducing transport of nitrogen-rich lighter parcels upward while CO<sub>2</sub>-rich  
175 heavier parcels would move downward. Additional experimental and theoretical studies are  
176 clearly needed to investigate this possibility and to solve this puzzle.

## 177 **Dynamics of the deep atmosphere of Venus**

178 To better understand the dynamical state of the different atmospheric layers, as well as the be-  
179 havior of the PBL near the surface of Venus, the atmospheric circulation was explored using the  
180 *Laboratoire de Meteorologie Dynamique* (LMD) Venus General Circulation Model (GCM).<sup>37</sup>  
181 The variation of the mean molecular mass with pressure in the deep atmosphere was imple-  
182 mented in the computation of the potential temperature within the GCM, though this modi-  
183 fication only slightly affects the dynamical state of the deepest layers. Fitting the observed  
184 temperature structure in detail with a radiative transfer model is challenging, because of the  
185 sensitivity of the temperature profile to many parameters that are not well known.<sup>38</sup> However,

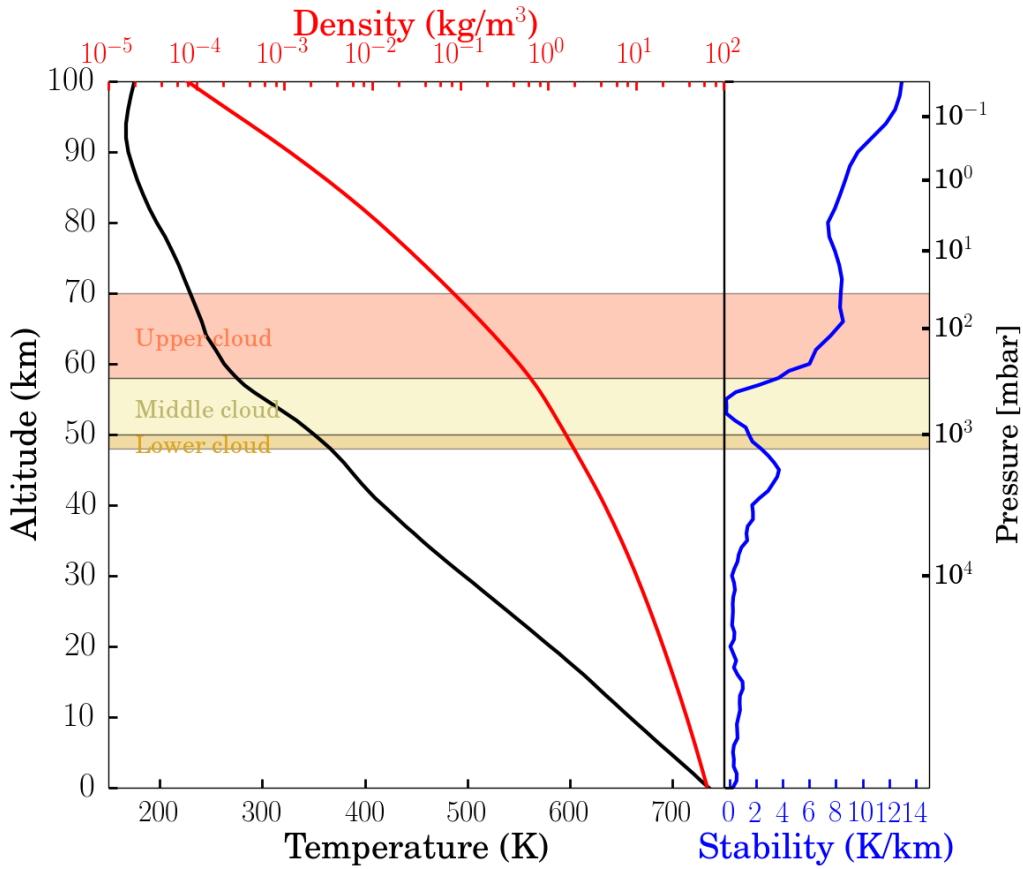
186 with a fine tuning of these parameters (detailed in the online Methods section), the GCM is able  
187 to reproduce the vertical structure of the potential temperature. Therefore, the mean meridional  
188 circulation and the turbulent activity diagnosed by the GCM (Fig. 4) can be used to evaluate the  
189 dynamical conditions within the atmosphere, including the deepest layer discussed here, despite  
190 the large difficulty to get observational constraints for this region.

191 The deepest layer (below 8 km) is close to neutral stability. In the simulation, it is slightly  
192 turbulent only near its top, and near the surface with a diurnal convective layer that reaches 1  
193 to 2 km above the surface around noon local time. This result of the GCM radiative transfer  
194 is obtained both when taking into account the composition variation and when composition is  
195 uniform. The mean meridional circulation participates in the mixing of the energy through a  
196 surface Hadley-type cell roughly 7-km thick. This is similar to the 2-km thick seasonal PBL  
197 observed on Titan by the Huygens probe, associated with the mixing by the deepest mean  
198 meridional circulation cells.<sup>39</sup> The hypothetical separation of N<sub>2</sub> and CO<sub>2</sub> that would explain the  
199 VeGa-2 potential temperature profile in the deepest layer needs to occur on timescales shorter  
200 than the dynamical overturning of this surface cell ( $\tau_{dyn} = L/\bar{v}$ , where  $L \sim 10^4$  km is the  
201 horizontal size of the cell and  $\bar{v} \sim 0.05$  m/s is the mean meridional wind near the surface,  
202 yielding  $\tau_{dyn} \sim 2 \times 10^8$  s, or 20 Vd) in order to maintain this vertical gradient in the atmospheric  
203 composition, while the layer is close to convective instability. The simulation confirms the very  
204 small spatial and temporal variations of the temperature profile, with a diurnal cycle only active  
205 near the surface.

## 206 **Dense gas separation at Venus and beyond**

207 The unexplained behavior of the CO<sub>2</sub>/N<sub>2</sub> mixture in the temperature and pressure conditions  
208 of the deep atmosphere of Venus needs to be confirmed. First, it illustrates how important it  
209 is to go back to Venus to make additional in-situ measurements down to the surface. Second,

210 further studies are needed, both theoretical and experimental. The compositional gradient de-  
211 duced from our interpretation of the VeGa-2 profile (5 ppm/m) could be measured in a large  
212 experimental tank where Venus' atmospheric conditions can be reproduced. Such a result could  
213 trigger interest for theoretical and experimental studies dedicated to other binary mixtures, that  
214 could be relevant for the high-pressure atmospheres of giant planets of our own solar system, or  
215 for extra-solar planets.



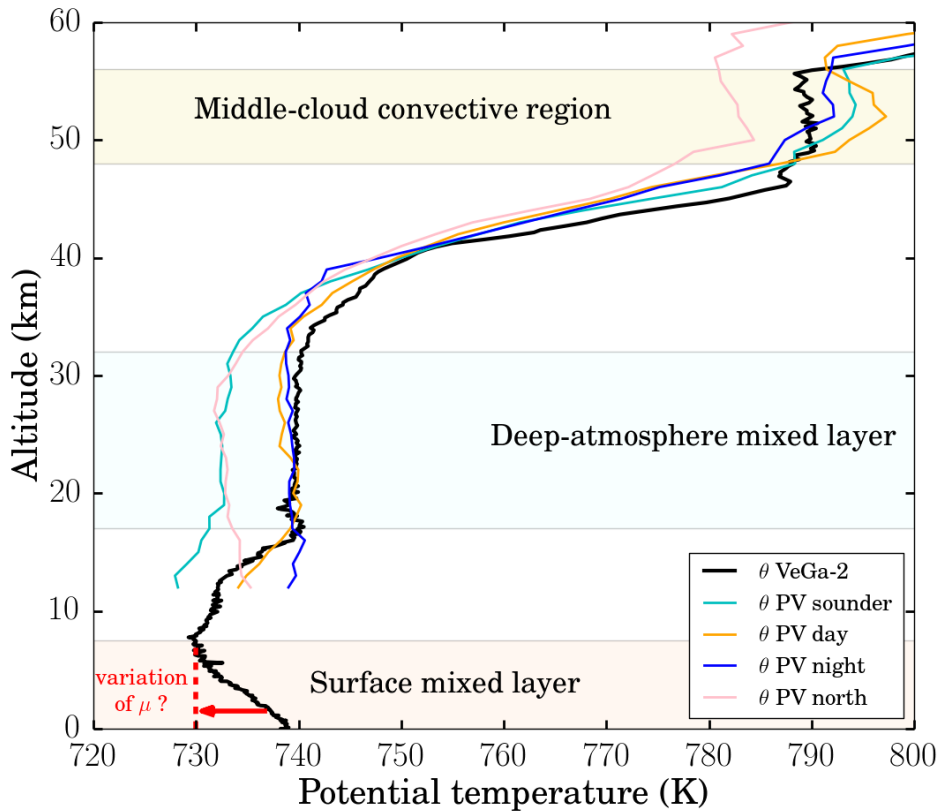
216

217 **Figure 1 | Vertical structure of the atmosphere of Venus.** Vertical profiles, as a function of  
 218 altitude and pressure, of the temperature, density and static stability (i.e., the difference between  
 219 the vertical gradient of temperature and the adiabatic lapse rate), from the Venus International  
 220 Reference Atmosphere model.<sup>22</sup> Cloud layers are also indicated.



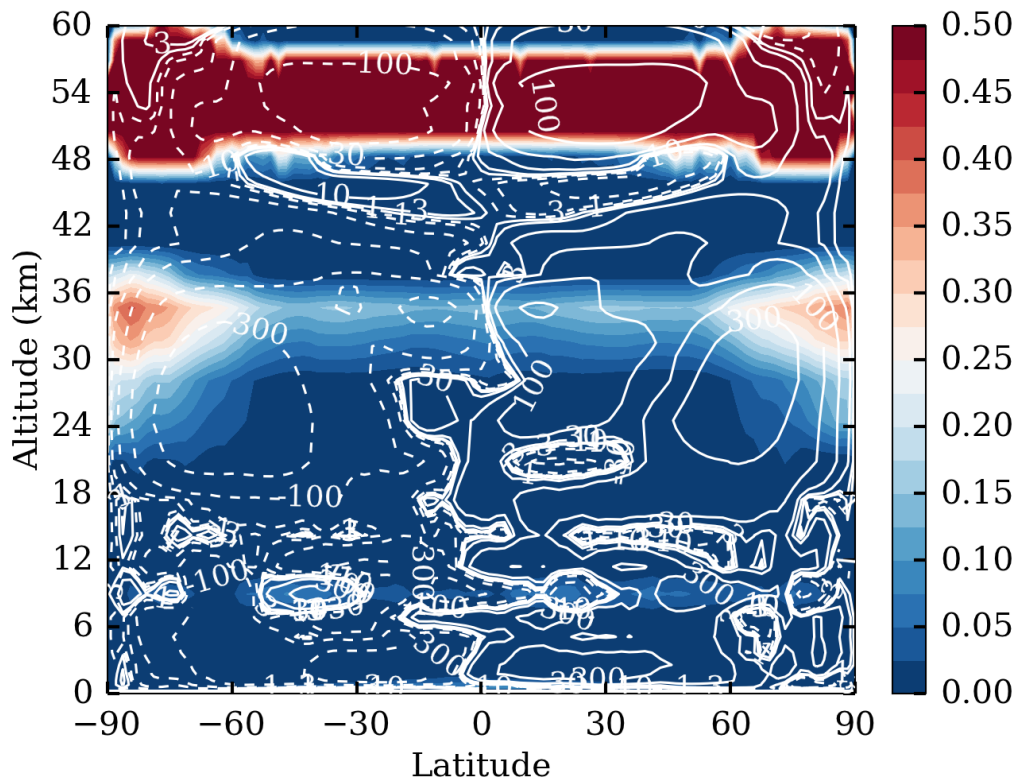
221

222 **Figure 2 | The VeGa-2 spacecraft.** Model of the VeGa spacecraft, with the lander visible in the  
223 top spherical shell (Lavochkin Museum, near Moscow). Image credits: Lavochkin Association.



224

225 **Figure 3 | Vertical profile of potential temperature  $\theta$  computed from temperatures mea-**  
 226 **sured by VeGa-2.** Potential temperature is computed using Eq. S10 in the online Methods.  
 227 VeGa-2 profile shows the convective layer present in the middle and lower clouds (48-56 km al-  
 228 titude), observed in all in-situ and radio-occultation datasets,<sup>14,22</sup> as well as a deep-atmosphere  
 229 mixed layer (17-32 km altitude), consistent with the Venus International Reference Atmosphere  
 230 (VIRA) model<sup>22</sup> and the Pioneer Venus Sounder, Day and Night probes.<sup>16</sup> The highly unstable  
 231 7-km thick surface layer is also highlighted ( $\mu$  is the mean molecular mass of the atmosphere).



232

233 **Figure 4 | Meridional distributions of the turbulent mixing coefficient and averaged stream**  
 234 **function.** The diurnal and zonal average of the turbulent mixing coefficient  $K_z$  diagnosed in  
 235 the GCM is shown with colors (unit is  $\text{m}^2/\text{s}$ ), showing convective regions, while the mean  
 236 meridional circulation is illustrated by the averaged stream function with the white contours  
 237 (unit is  $10^9 \text{ kg/s}$ ). The amplitude of  $K_z$  reaches more than  $10 \text{ m}^2/\text{s}$  in the cloud turbulent layer  
 238 (48-57 km).

## 239 **Box 1**

240 The stability of an atmospheric region is assessed by moving adiabatically an air parcel along the  
241 vertical. For an ideal gas, its temperature follows the adiabatic lapse rate  $\left(\frac{dT}{dz}\right)_{adiab} = \Gamma = -\frac{g}{c_p}$ ,  
242 where  $g$  is the gravity and  $c_p$  is the specific heat capacity at constant pressure. In a well mixed  
243 atmosphere (constant molecular mass  $\mu$ ), if the parcel rises to a colder environment (or sinks  
244 to a warmer environment), it will continue to rise (or sink), becoming buoyant and triggering  
245 convective activity. This corresponds to a vertical temperature gradient lower than the adiabatic  
246 lapse rate. The stability can then be assessed with the static stability:  $S = \frac{dT}{dz} - \Gamma$ : when  $S$  is  
247 positive, the atmosphere is stable, but when  $S$  is negative, convective activity will mix energy  
248 and modify the temperature profile until  $S = 0$ .

249 The potential temperature  $\theta$  is defined as the temperature that an air parcel would get after  
250 undergoing an adiabatic displacement from its position  $(T, p)$  to a reference pressure  $p_{ref}$ . The  
251 static stability  $S$  is equivalent to the vertical gradient of the potential temperature,  $\frac{1}{\theta} \frac{d\theta}{dz}$ .

252 When the mean molecular mass is not constant with altitude, to define the buoyancy of a  
253 given parcel, the relevant variable is the potential density  $\rho_\theta$ , defined as the density a parcel with  
254 the density  $\rho(\mu, T, p)$  would have when displaced adiabatically (and with constant composition)  
255 to the reference pressure  $p_{ref}$ ,  $\rho_\theta(\mu, \theta, p_{ref})$ . In the case of the deep atmosphere of Venus, the  
256 stability criterion can be reduced to the usual criterion, but applied to the modified potential  
257 temperature  $\theta' = \theta(\mu_{ref}/\mu)$ , with  $\mu_{ref} = 43.44$  g/mol a reference value corresponding to CO<sub>2</sub>  
258 mixed with 3.5% of N<sub>2</sub>:  $\frac{1}{\theta'} \frac{d\theta'}{dz} \geq 0$ .

259 Additional details may be found in the online Methods section.



## References

- 261 1. Crisp, D. & Titov, D. The thermal balance of the Venus atmosphere. In S. W. Bougher,  
262 D. M. Hunten and R. J. Phillips (ed.) *Venus II, geology, geophysics, atmosphere, and solar*  
263 *wind environment*, 353–384 (Univ. of Arizona Press, 1997).
- 264 2. von Zahn, U., Kumar, S., Niemann, H. & Prinn, R. Composition of the Venus atmosphere.  
265 In D. M. Hunten, L. Colin, T. M. Donahue and V. I. Moroz (ed.) *Venus*, 299–430 (Univ. of  
266 Arizona Press, 1983).
- 267 3. Taylor, F. W., Crisp, D. & Bézard, B. Near-infrared sounding of the lower atmosphere  
268 of Venus. In S. W. Bougher, D. M. Hunten and R. J. Phillips (ed.) *Venus II, geology,*  
269 *geophysics, atmosphere, and solar wind environment*, 325–351 (Univ. of Arizona Press,  
270 1997).
- 271 4. de Bergh, C. *et al.* The composition of the atmosphere of Venus below 100km altitude: An  
272 overview. *Planet. & Space Sci.* **54**, 1389–1397 (2006).
- 273 5. Esposito, L. W., Knollenberg, R. G., Marov, M. I., Toon, O. B. & Turco, R. P. *The clouds*  
274 *and hazes of Venus*, 484–564 (Univ. of Arizona Press, 1983).
- 275 6. Oertel, D. *et al.* Infrared spectrometry of Venus from Venera-15 and Venera-16. *Adv. Space*  
276 *Res.* **5**, 25–36 (1985).
- 277 7. Moroz, V. I., Linkin, V. M., Matsygorin, I. A., Spaenkuch, D. & Doehler, W. Venus space-  
278 craft infrared radiance spectra and some aspects of their interpretation. *Appl. Opt.* **25**,  
279 1710–1719 (1986).

- 280 8. Yakovlev, O. I., Matyugov, S. S. & Gubenko, V. N. Venera-15 and -16 middle atmosphere  
281 profiles from radio occultations: Polar and near-polar atmosphere of Venus. *Icarus* **94**,  
282 493–510 (1991).
- 283 9. Kliore, A. J. & Patel, I. R. Vertical structure of the atmosphere of Venus from Pioneer  
284 Venus orbiter radio occultations. *J. Geophys. Res.* **85**, 7957–7962 (1980).
- 285 10. Taylor, F. W. *et al.* Structure and meteorology of the middle atmosphere of Venus: Infrared  
286 remote sounding from the Pioneer Orbiter. *J. Geophys. Res.* **85**, 7963–8006 (1980).
- 287 11. Hinson, D. P. & Jenkins, J. M. Magellan radio occultation measurements of atmospheric  
288 waves on Venus. *Icarus* **114**, 310–327 (1995).
- 289 12. Drossart, P. *et al.* Scientific goals for the observation of Venus by VIRTIS on ESA/Venus  
290 Express mission. *Planet. & Space Sci.* **55**, 1653–1672 (2007).
- 291 13. Bertaux, J.-L. *et al.* SPICAV on Venus Express: Three spectrometers to study the global  
292 structure and composition of the Venus atmosphere. *Planet. & Space Sci.* **55**, 1673–1700  
293 (2007).
- 294 14. Tellmann, S., Pätzold, M., Hausler, B., Bird, M. K. & Tyler, G. L. Structure of the Venus  
295 neutral atmosphere as observed by the radio science experiment VeRa on Venus Express.  
296 *J. Geophys. Res.* **114**, E00B36 (2009).
- 297 15. Keldysh, M. V. Venus exploration with the Venera 9 and Venera 10 spacecraft. *Icarus* **30**,  
298 605–625 (1977).
- 299 16. Seiff, A. *et al.* Measurements of thermal structure and thermal contrasts in the atmosphere  
300 of Venus and related dynamical observations - Results from the four Pioneer Venus probes.  
301 *J. Geophys. Res.* **85**, 7903–7933 (1980).

- 302 17. Linkin, V. M. *et al.* Vertical thermal structure in the Venus atmosphere from provisional  
303 Vega 2 temperature and pressure data. *Sov. Astron. Lett.* **12**, 40–42 (1986).
- 304 18. Linkin, V. M., Blamont, J., Deviatkin, S. I., Ignatova, S. P. & Kerzhanovich, V. V. Ther-  
305 mal structure of the Venus atmosphere according to measurements with the Vega-2 lander.  
306 *Kosm. Issled.* **25**, 659–672 (1987).
- 307 19. Bezdard, B., de Bergh, C., Crisp, D. & Maillard, J.-P. The deep atmosphere of Venus re-  
308 vealed by high-resolution nightside spectra. *Nature* **345**, 508–511 (1990).
- 309 20. Pollack, J. B. *et al.* Near-infrared light from Venus’ nightside - A spectroscopic analysis.  
310 *Icarus* **103**, 1–42 (1993).
- 311 21. Meadows, V. S. & Crisp, D. Ground-based near-infrared observations of the Venus night-  
312 side: The thermal structure and water abundance near the surface. *J. Geophys. Res.* **101**,  
313 4595–4622 (1996).
- 314 22. Seiff, A., Schofield, J. T., Kliore, A. J. *et al.* Model of the structure of the atmosphere of  
315 Venus from surface to 100 km altitude. *Adv. Space Res.* **5**, 3–58 (1985).
- 316 23. Zasova, L. V., Ignatiev, N. I., Khatuntsev, I. A. & Linkin, V. Structure of the Venus atmo-  
317 sphere. *Planet. & Space Sci.* **55**, 1712–1728 (2007).
- 318 24. Hoffman, J. H., Oyama, V. I. & von Zahn, U. Measurement of the Venus lower atmosphere  
319 composition - A comparison of results. *J. Geophys. Res.* **85**, 7871–7881 (1980).
- 320 25. von Zahn, U. & Moroz, V. Composition of the Venus atmosphere below 100 km altitude.  
321 *Adv. Sp. Res.* **5**, 173–195 (1985).
- 322 26. Avduevskii, V. S. *et al.* Automatic stations Venera 9 and Venera 10 - Functioning of descent  
323 vehicles and measurement of atmospheric parameters. *Cosmic Res.* **14**, 655–666 (1977).

- 324 27. Zasova, L. V., Moroz, V. I., Linkin, V. M., Khatuntsev, I. V. & Maiorov, B. S. Structure of  
325 the Venusian atmosphere from surface up to 100 km. *Cosmic Res.* **44**, 364–383 (2006).
- 326 28. Seiff, A. & the VEGA Balloon Science Team. Further information on structure of the  
327 atmosphere of Venus derived from the VEGA Venus Balloon and Lander mission. *Adv.*  
328 *Space Res.* **7**, 323–328 (1987).
- 329 29. Gierasch, P. J. *et al.* The general circulation of the Venus atmosphere: an assessment.  
330 In S. W. Bougher, D. M. Hunten and R. J. Phillips (ed.) *Venus II, geology, geophysics,*  
331 *atmosphere, and solar wind environment*, 459–500 (Univ. of Arizona Press, 1997).
- 332 30. Hendry, D. *et al.* Exploration of high pressure equilibrium separations of nitrogen and  
333 carbon dioxide. *J. CO<sub>2</sub> Utilization* **3-4**, 37–43 (2013).
- 334 31. Spiga, A., Forget, F., Lewis, S. R. & Hinson, D. P. Structure and dynamics of the convec-  
335 tive boundary layer on Mars as inferred from large-eddy simulations and remote-sensing  
336 measurements. *Q. J. R. Meteorol. Soc.* **136**, 414–428 (2010).
- 337 32. Read, P. L. *et al.* Global energy budgets and ‘Trenberth diagrams’ for the climates of  
338 terrestrial and gas giant planets. *Quater. J. R. Met. Soc.* **142**, 703–720 (2016).
- 339 33. Wordsworth, R. D. Atmospheric nitrogen evolution on Earth and Venus. *Earth and Planet.*  
340 *Sci. Lett.* **447**, 103–111 (2016).
- 341 34. Espanani, R., Miller, A., Busick, A., Hendry, D. & Jacoby, W. Separation of N<sub>2</sub>/CO<sub>2</sub>  
342 mixture using a continuous high-pressure density-driven separator. *J. CO<sub>2</sub> Utilization* **14**,  
343 67–75 (2016).

- 344 35. Span, R. & Wagner, W. A New Equation of State for Carbon Dioxide Covering the Fluid  
345 Region from the Triple-Point Temperature to 1100 K at Pressures up to 800 MPa. *J. Phys.*  
346 *Chem. Ref. Data* **25**, 1509–1596 (1996).
- 347 36. Landau, L. D. & Lifshitz, E. M. *Course of Theoretical Physics vol. 6: Fluid mechanics*  
348 (Pergamon Press, Oxford, UK, 1959).
- 349 37. Lebonnois, S., Sugimoto, N. & Gilli, G. Wave analysis in the atmosphere of Venus below  
350 100-km altitude, simulated by the LMD Venus GCM. *Icarus* **278**, 38–51 (2016).
- 351 38. Lebonnois, S., Eymet, V., Lee, C. & Vatan d’Ollone, J. Analysis of the radiative budget  
352 of Venus atmosphere based on infrared Net Exchange Rate formalism. *J. Geophys. Res.*  
353 *Planets* **120**, 1186–1200 (2015).
- 354 39. Charnay, B. & Lebonnois, S. Two boundary layers in Titan’s lower troposphere inferred  
355 from a climate model. *Nature Geosci.* **5**, 106–109 (2012).

## 356 **Acknowledgements**

357 The authors thank Ludmila Zasova for providing the VeGa-2 probe temperature profile, and  
358 Josette Bellan for mentioning barodiffusion and useful discussion on this phenomenon. S.L.  
359 acknowledges the support of the Centre National d’Etudes Spatiales. G.S. acknowledges the  
360 support of the Keck Institute for Space Studies under the project ”Techniques and technologies  
361 for investigating the interior structure of Venus”.

## 362 **Methods**

### 363 **Stability and potential temperature**

364 The stability of an air parcel undergoing an adiabatic displacement in situations where  $\mu$  and/or  
365  $c_p$  may depend on altitude, pressure or temperature is detailed in the following study. The  
366 notations used are as follows:  $R$  is the universal gas constant ( $R=8.3144621 \text{ J mol}^{-1}\text{K}^{-1}$ ),  $\mu$  is  
367 the mean molecular mass,  $p$  is the pressure,  $\rho$  is the density,  $v = 1/\rho$  is the specific volume,  $T$   
368 is the temperature,  $c_p$  and  $c_v$  are the specific heat capacities at constant pressure and constant  
369 volume,  $\lambda = c_p/c_v$  and  $\kappa = R/(\mu c_p)$ .

370 **Initial equations.** The basic equations for this study are:

371 - the specific heat relations

372 (Eq. S1)

$$dU = c_v dT$$

373 (Eq. S2)

$$\frac{R}{\mu} = c_p - c_v$$

374 which yields

$$\kappa = 1 - \frac{1}{\lambda}$$

375 - the first law of thermodynamics for adiabatic displacement

376 (Eq. S3)

$$dU = -pdv$$

377 - the equation of state for an ideal gas

378 (Eq. S4)

$$\rho = \frac{\mu p}{RT}$$

379 Note that in the case of the deep atmosphere of Venus, the ideal gas law is only an approxi-  
380 mation, but with an error on density less than 0.8% (Table S1).<sup>19,35</sup>

381 - the hydrostatic balance

382 (Eq. S5)

$$dp = -\rho g dz$$

383 **When  $\mu$  is constant in the atmosphere.** In the cases where  $\mu$  is constant in the atmosphere,

384 Eq. S4 can be written as:

$$pv = \frac{R}{\mu} T$$

385 Differentiating this equation yields

386 (Eq. S6)

$$p dv + v dp = \frac{R}{\mu} dT$$

387 From Eqs. S1 and S3, we get

$$p dv = -c_v dT$$

388 Together with Eq. S2, Eq. S6 becomes

$$v dp = c_p dT$$

389 Using Eq. S4 again, this yields

390 (Eq. S7)

$$\frac{R}{\mu} \frac{dp}{p} = c_p \frac{dT}{T}$$

391 The potential temperature  $\theta$  is defined as the temperature that an air parcel would get after  
392 undergoing an adiabatic displacement to a reference pressure  $p_{ref}$ . Its expression is obtained  
393 by integrating this adiabatic displacement from  $(T, p)$  to  $(\theta, p_{ref})$ . When  $c_p$  is constant, Eq. S7  
394 yields the usual expression

395 (Eq. S8)

$$\theta = T \left( \frac{p_{ref}}{p} \right)^\kappa$$

396 When  $c_p$  depends on the temperature, the integration is not direct. Using the expression

397 (Eq. S9)

$$c_p = c_{p0} \left( \frac{T}{T_0} \right)^\nu$$

398 (with  $c_{p0}=1000$  J/kg/K,  $T_0 = 460$  K and  $\nu = 0.35$  for Venus' atmosphere),<sup>35,40,41</sup> it can be  
399 demonstrated<sup>40</sup> that the new expression for  $\theta$  is:

400 (Eq. S10)

$$\theta^\nu = T^\nu + \nu T_0^\nu \ln \left( \frac{p_{ref}}{p} \right)^{\kappa_0}$$

401 with  $\kappa_0 = R/(\mu c_{p0})$ .

402 Using Eqs. S4, S5 and S7 yields

$$-\frac{g dz}{T} = c_p \frac{dT}{T}$$

403 which gives the adiabatic lapse rate (valid even for variable  $c_p$ )

404 (Eq. S11)

$$\left( \frac{dT}{dz} \right)_{adiab} = \Gamma = -\frac{g}{c_p}$$

405 **When  $\mu$  depends on altitude, pressure or temperature.** The stability criterion is established  
406 as follows.<sup>42,43</sup> Consider a parcel that is displaced adiabatically on an elemental distance  $dz$ ,  $q^*$   
407 refers to the variable  $q$  in the parcel.

408 Eq. S4 can be written as

$$p^* \mu^* = \rho^* R T^*$$

409 Taking the logarithm then differentiating along the vertical axis ( $\mu^*$  is constant because the  
410 composition of the parcel does not change) yields

$$\frac{1}{p^*} \frac{dp^*}{dz} = \frac{1}{\rho^*} \frac{d\rho^*}{dz} + \frac{1}{T^*} \frac{dT^*}{dz}$$



411 Using Eq. S7 applied to the parcel and  $p = p^*$  yields

412 (Eq. S12)

$$\frac{1}{\rho^*} \frac{d\rho^*}{dz} = \frac{1}{p} \frac{dp}{dz} (1 - \kappa^*)$$

413 with  $\kappa^* = R/(\mu^*c_p)$ .

414 For the background gas, Eq. S4 can be written as:

$$\rho = \frac{\mu p}{RT}$$

415 Taking the logarithm then differentiating along the vertical axis yields

416 (Eq. S13)

$$\frac{1}{\rho} \frac{d\rho}{dz} = \frac{1}{\mu} \frac{d\mu}{dz} + \frac{1}{p} \frac{dp}{dz} - \frac{1}{T} \frac{dT}{dz}$$

417 The stability criterion is

418 (Eq. S14)

$$\frac{1}{\rho^*} \frac{d\rho^*}{dz} > \frac{1}{\rho} \frac{d\rho}{dz}$$

419 Eqs. S12 and S13 yield

420 (Eq. S15)

$$\frac{1}{\mu} \frac{d\mu}{dz} - \frac{1}{T} \frac{dT}{dz} + \frac{\kappa^*}{p} \frac{dp}{dz} < 0$$

421 Applying this stability criterion, the adiabatic lapse rate is obtained when neutral for stabil-

422 ity:

423 (Eq. S16)

$$\frac{1}{\mu} \frac{d\mu}{dz} - \frac{1}{T} \frac{dT}{dz} + \frac{\kappa^*}{p} \frac{dp}{dz} = 0$$

424 Using Eqs. S4, S5 and the fact that  $\kappa/\kappa^*$  tends to 1 for an elemental displacement, this can

425 be written as

426 (Eq. S17)

$$\left( \frac{dT}{dz} \right)_{adiab} = \Gamma = \frac{T}{\mu} \frac{d\mu}{dz} - \frac{g}{c_p}$$

427 which is valid even for variable  $c_p$ .

428 To define the buoyancy of a given parcel, the relevant variable is the potential density  $\rho_\theta$ ,  
 429 defined as the density a parcel with the density  $\rho(\mu, T, p)$  would have when displaced adiabatically  
 430 ically (and with constant composition) to the reference pressure  $p_{ref}$ ,  $\rho_\theta(\mu, \theta, p_{ref})$ . Using the  
 431 ideal gas law (Eq. S4), the potential density is

432 (Eq. S18)

$$\rho_\theta = \frac{\mu p_{ref}}{R\theta} = \frac{\mu_{ref} p_{ref}}{R\theta'}$$

433 with the modified potential temperature  $\theta'$  defined by

434 (Eq. S19)

$$\theta' = \theta(\mu_{ref}/\mu)$$

435 Due to the variation of  $\mu$  with altitude and the dependence of  $\theta$  on  $\mu$ , it is not correct to  
 436 reduce the stability criterion (Eq. S16) to the usual criterion, i.e., the direct comparison of the  
 437 potential density between two atmospheric levels.<sup>44</sup>

438 (Eq. S20)

$$\frac{1}{\rho_\theta} \frac{d\rho_\theta}{dz} = \frac{1}{\mu} \frac{d\mu}{dz} - \left( \frac{1}{\theta} \frac{\partial\theta}{\partial z} \right)_\mu - \left( \frac{1}{\theta} \frac{\partial\theta}{\partial\mu} \right)_z \frac{d\mu}{dz}$$

439 For an elemental displacement, the definition of  $\theta$  yields

440 (Eq. S21)

$$\left( \frac{1}{\theta} \frac{\partial\theta}{\partial z} \right)_\mu = \frac{1}{T} \frac{dT}{dz} - \frac{\kappa^*}{p} \frac{dp}{dz}$$

441 which can be inserted in Eq. S20 to give

442 (Eq. S22)

$$\frac{1}{\rho_\theta} \frac{d\rho_\theta}{dz} = \frac{1}{\mu} \frac{d\mu}{dz} - \frac{1}{T} \frac{dT}{dz} + \frac{\kappa^*}{p} \frac{dp}{dz} - \left( \frac{1}{\theta} \frac{\partial\theta}{\partial\mu} \right)_z \frac{d\mu}{dz}$$

443 Eq. S22 shows that  $d\rho_\theta/dz = 0$  (or  $d\theta'/dz = 0$ ) is not equivalent to the stability criterion  
 444 (Eq. S16), unless the last term of the right side is negligible against the first.

445 However, in the case of the deep atmosphere of Venus, the vertical profile of  $\theta(\mu)$  is very  
 446 close (difference less than 0.15 K everywhere) to the profile of  $\theta(\mu_{ref})$ , with  $\mu_{ref} = 43.44$  g/mol  
 447 a reference value corresponding to CO<sub>2</sub> mixed with 3.5% of N<sub>2</sub>. This yields  $(\mu/\theta)(\partial\theta/\partial\mu) \sim$   
 448  $(43.44/735) \times (0.15/0.56) \sim 0.016$ , much smaller than 1. It is therefore a good approximation  
 449 to consider that the definition of the potential temperature  $\theta$  is not dependent on the initial mean  
 450 molecular mass of the air parcel, i.e.,  $\partial\theta/\partial\mu = 0$  at any given level. In this case, the stability  
 451 criterion is equivalent to the usual criterion applied to the modified potential temperature  $\theta'$ :

452 (Eq. S23)

$$\frac{1}{\theta'} \frac{d\theta'}{dz} = 0.$$

### 453 Radiative transfer details

454 In the GCM used for our study, the temperature structure is modeled using a full radiative  
 455 transfer model. In the infrared range, net exchange rate (NER) formalism is used<sup>38,45</sup> based  
 456 on up-to-date gas opacities including collision-induced absorption from CO<sub>2</sub> dimers<sup>46</sup>, and the  
 457 most recent cloud model deduced from Venus-Express datasets<sup>47</sup>. In the solar range, vertical  
 458 profiles of the solar fluxes computed using this new cloud model are used, depending on lati-  
 459 tude and solar zenith angle<sup>48</sup>. As discussed in a recent work<sup>38</sup> extinction coefficients below the  
 460 clouds in windows located between 3 and 7 microns play a key role in shaping the deep atmo-  
 461 sphere temperature profile. The solar heating profile below the clouds is also crucial, though it  
 462 is poorly constrained by available data.

463 Globally averaged 1-dimensional simulations were performed to assess the sensitivity to  
 464 crucial hypotheses in the radiative transfer calculation. Different solar heating rate models were  
 465 used<sup>48–50</sup> (Fig. S1a). The composition of the lower haze particles, located between the cloud  
 466 base (48 km) and 30 km and observed by the probe nephelometers<sup>51</sup>, is not established, so their  
 467 optical properties are not well constrained. The absorption of the solar flux in this region is

468 therefore subject to uncertainty. An increased solar absorption (by a factor 3) in this region in  
469 the H15 profile<sup>48</sup> (Fig. S1) provides the best fit to the VIRA and Vega-2 temperature profiles.  
470 In the infrared, some additional extinction is needed below the clouds in the 3 to 7 microns  
471 wavelength range to fit the temperature profile in the stable region below the clouds<sup>38</sup>. The  
472 lower haze, which is not taken into account in the reference NER computations, can contribute  
473 to this small additional continuum. The impact of several hypotheses on this additional opacity  
474 is illustrated in Fig. S1b. The best fit to the VIRA and Vega-2 temperature profiles is obtained  
475 with an additional extinction of  $1.3 \times 10^{-6} \text{ cm}^{-1} \text{ amagat}^{-2}$  in the lower haze region (30-48 km),  
476 and of  $4 \times 10^{-7} \text{ cm}^{-1} \text{ amagat}^{-2}$  in the region between 30 and 16 km, where a transition from  
477 instability to stability against convection is observed in the Vega-2 profile, but also in the Pioneer  
478 Venus Sounder, Day and Night probes at similar altitudes (15 to 20 km)<sup>19</sup>.

## 479 **References**

- 480 40. Lebonnois, S. *et al.* Superrotation of Venus' atmosphere analysed with a full General  
481 Circulation Model. *J. Geophys. Res.* **115**, E06006 (2010).
- 482 41. Poling, B., Prausnitz, J. & O'Connell, J. *The properties of gases and liquids* (McGraw-Hill,  
483 2001).
- 484 42. Ledoux, P. Stellar models with convection and with discontinuity of the mean molecular  
485 weight. *Astrophys. J.* **105**, 305–321 (1947).
- 486 43. Hess, S. L. Static stability and thermal wind in an atmosphere of variable composition:  
487 Applications to Mars. *J. Geophys. Res.* **84**, 2969–2973 (1979).
- 488 44. Pierrehumbert, R. T. *Principles of Planetary Climate* (Cambridge Univ. Press, Cambridge,  
489 UK, 2010).

- 490 45. Eymet, V. *et al.* Net-exchange parameterization of the thermal infrared radiative transfer  
491 in Venus' atmosphere. *J. Geophys. Res.* **114**, E11008 (2009).
- 492 46. Stefani, S., Piccioni, G., Snels, M., Grassi, D. & Adriani, A. Experimental CO<sub>2</sub> absorption  
493 coefficients at high pressure and high temperature. *J. of Quantit. Spec. and Rad. Transfer*  
494 **117**, 21–28 (2013).
- 495 47. Haus, R., Kappel, D. & Arnold, G. Atmospheric thermal structure and cloud features in the  
496 southern hemisphere of Venus as retrieved from VIRTIS/VEX radiation measurements.  
497 *Icarus* **232**, 232–248 (2014).
- 498 48. Haus, R., Kappel, D. & Arnold, G. Radiative heating and cooling in the middle and  
499 lower atmosphere of Venus and responses to atmospheric and spectroscopic parameter  
500 variations. *Planet. & Space Sci.* **117**, 262–294 (2015).
- 501 49. Crisp, D. Radiative forcing of the Venus mesosphere. I - Solar fluxes and heating rates.  
502 *Icarus* **67**, 484–514 (1986).
- 503 50. Lee, C. & Richardson, M. I. A Discrete Ordinate, Multiple Scattering, Radiative Transfer  
504 Model of the Venus Atmosphere from 0.1 to 260 $\mu$ m. *J. Atm. Sci.* **68**, 1323–1339 (2011).
- 505 51. Knollenberg, R. G. *et al.* The clouds of Venus: A synthesis report. *J. Geophys. Res.* **85**,  
506 8059–8081 (1980).

## 507 **Data and code availability**

508 The VeGa-2 temperature profile was kindly provided by Ludmila Zasova. It is avail-  
509 able from the corresponding author upon request.

510 The LMD Venus GCM used in this study is developed in the corresponding author's team.  
511 It is also available upon request.

512 **Author contributions**

513 Both authors contributed equally to the manuscript.

514 **Additional information**

515 Methods section and Supplementary Information are available in the online version of the paper.

516 Correspondence and requests for materials should be addressed to S.L.

517 **Competing financial interests**

518 The authors declare no competing financial interests.